Scientific Research Publishing

International Journal of Astronomy and Astrophysics, 2019, 9, 368-392
https://www.scirp.org/journal/ijaa
ISSN Online: 2161-4725
ISSN Print: 2161-4717

Simulations and Measurements of Warm Dark Matter Free-Streaming and Mass

Bruce Hoeneisen

Universidad San Francisco de Quito, Quito, Ecuador
Email: bhoeneisen@usfq.edu.ec

How to cite this paper: Hoeneisen, B. (2019) Simulations and Measurements of Warm Dark Matter Free-Streaming and Mass. *International Journal of Astronomy and Astrophysics*, **9**, 368-392.
https://doi.org/10.4236/ijaa.2019.94026

Received: October 29, 2019
Accepted: December 8, 2019
Published: December 11, 2019

Abstract

We compare simulated galaxy distributions in the cold ΛCDM and warm ΛWDM dark matter models. The ΛWDM model adds one parameter to the ΛCDM model, namely the cut-off wavenumber k_{fs} of linear density perturbations. The challenge is to measure k_{fs}. This study focuses on "smoothing lengths" π/k_{fs} in the range from 12 Mpc to 1 Mpc. The simulations reveal two distinct galaxy populations at any given redshift z: *hierarchical galaxies* that form bottom up starting at the transition mass M_{fs}, and *stripped down galaxies* that lose mass to neighboring galaxies during their formation, are near larger galaxies, often have filamentary distributions, and seldom fill voids. We compare simulations with observations, and present four independent measurements of k_{fs}, and the mass m_h of dark matter particles, based on the redshift of first galaxies, galaxy mass distributions, and rotation curves of spiral galaxies.

Keywords

Dark Matter Mass, Warm Dark Matter Free-Streaming, Galaxy Mass Distribution, Spiral Galaxy Adiabatic Invariant

1. Introduction

The cold dark matter ΛCDM model is apparently in agreement with all current observations on scales greater than 10 Mpc, with only six parameters and a few *ansatz*, e.g. $\Omega_k = 0$ and Ω_Λ constant [1]. However, at scales less than 10 Mpc, there appear to be discrepancies with observations, known as the "small scale crisis" (missing satellites, too big to fail, core vs. cusp, voids, dwarf galaxy distribution, dark matter adiabatic invariant, etc.) [2]. A modification of the ΛCDM model, proposed to address these issues, is warm dark matter (ΛWDM), which assumes that the power spectrum of linear density perturbations $P(k)$ becomes suppressed for comoving wavenumbers $k > k_{fs}$, due to free-streaming of dark matter particles that become non-relativistic while the universe is still dominated by radiation. For the current status of warm dark matter research, and a list of references, see [1] and [2]. The challenge is to measure, or constrain, the cut-off wavenumber k_{fs}. To this end, we present a comparison of galaxy distributions in the cold and warm dark matter models with simulations. This study focuses on "smoothing lengths" π/k_{fs} in the range from 12 Mpc to 1 Mpc. Finally, we present four independent measurements of k_{fs}, and of the mass m_h of dark matter particles. These measurements are based on:

- The redshift of formation of first galaxies,
- The distributions of masses of Sloan Digital Sky Survey SDSS DR15 galaxies,
- Spiral galaxy rotation curves, and
- The assumption that dark matter was once in thermal and diffusive equilibrium with the Standard Model sector, and decoupled while still ultra-relativistic.

Finally, the results of these measurements are presented in **Table 2**.

Our notation and the values of cosmological parameters are as in Reference [1].

2. Warm Dark Matter

Let $P(k)$ be the power spectrum of linear density perturbations in the ΛCDM model as defined in Reference [3]. The normalization of $P(k)$ refers to the present time with expansion parameter $a \equiv 1$. $k = 2\pi/\lambda$ is the comoving wavenumber. The normalization of $P(k)$ is fixed, within uncertainties, by measurements of the Sachs-Wolfe effect in the range $-3.1 \lesssim \log_{10}(k/h\,\text{Mpc}^{-1}) \lesssim -2.7$, and by measurements of σ_8 in the range $-1.3 \lesssim \log_{10}(k/h\,\text{Mpc}^{-1}) \lesssim -0.6$ [1]. The Planck satellite measurements of the Cosmic Microwave Background fluctuations accurately determine $P(k)$ in the range $-3.5 < \log_{10}(k/h\,\text{Mpc}^{-1}) < -0.6$ corresponding to spherical harmonics with $3 < l < 2500$ [1].

We consider warm dark matter (ΛWDM) with a power spectrum of linear density perturbations suppressed by a factor α for $k > k_{fs}$. The suppression may be due to free-streaming, or to diffusion if elastic scattering between dark matter particles dominates over free-streaming, or to other causes. For warm dark matter, $\alpha \approx 0$. k_{fs} is the only new parameter for warm dark matter in addition to the parameters of the ΛCDM model. The transition mass corresponding to k_{fs} is $M_{fs} \equiv 4\pi R^3 \Omega_m \rho_{crit}/3$ with $R = 1.555/k_{fs}$ (the numerical factor 1.555 is obtained for a 3-dimensional Gaussian mass fluctuation, and its Fourier transform). For warm dark matter, the distribution of galaxy masses becomes suppressed by a factor β for $M < M_{fs}$ with respect to the cold dark matter case. β is a function of *k*.

3. Free-Streaming

We consider collisionless dark matter. The velocity of a dark matter particle at expansion parameter a has the form $v_h(a) = c\big/\sqrt{1+(a/a'_{h\text{NR}})^2}$. We consider the case $a'_{h\text{NR}} \lesssim a_{\text{eq}}/3$, *i.e.* warm dark matter. The comoving free-streaming distance of this particle until decoupling is

$$\begin{aligned} d_{\text{fs}} &= \int_0^{\text{dec}} \frac{v_h(a)\cdot \text{d}t}{a} = \int_0^{\text{dec}} \frac{c}{\sqrt{1+(a/a'_{h\text{NR}})^2}} \frac{\text{d}t}{a} \\ &= \eta \frac{c a'_{h\text{NR}}}{H_0}\left[\frac{1}{\sqrt{\Omega_r}} \ln\left(2\frac{a_{\text{eq}}}{a'_{h\text{NR}}}\right) + \frac{2}{\sqrt{\Omega_m}}\left(a_{\text{eq}}^{-1/2} - a_{\text{dec}}^{-1/2}\right)\right], \end{aligned} \tag{1}$$

where $\eta = 1$. The first term is the approximate integral from 0 to a_{eq}, and the second term is the approximate integral from a_{eq} to a_{dec}. A numerical integration obtains $\eta = 0.9118$.

If the free-streaming length d_{fs} were equal for all dark matter particles, $P(k)$ would not have a cut-off: only the amplitudes in $P(k)$ would change their phases without changing $P(k)$. It is approximately the standard deviation of d_{fs}, for the net distribution of density fluctuations, that obtains the cut-off wavenumber k_{fs}: $2\sigma(d_{\text{fs}}) = \lambda_{\text{fs}}/2 = \pi/k_{\text{fs}}$. We calculate $\sigma(d_{\text{fs}})$ with Equation (1) with

$$a'_{h\text{NR}} \equiv \frac{v_{h\text{rms}}(1)}{c}, \tag{2}$$

and $\eta = 0.2816$ to obtain the root-mean-square $\sigma(d_{\text{fs}}) \equiv \sqrt{\left\langle \left(d_{\text{fs}} - \langle d_{\text{fs}}\rangle\right)^2\right\rangle}$ over the distribution of the net density perturbations for an ideal gas (*i.e.* the distribution for temperature $T_h + \epsilon$ minus the distribution for temperature T_h [4]), or $\eta = 0.2628$ for a gas of fermions with zero chemical potential, or $\eta = 0.4115$ for a gas of bosons with zero chemical potential. In the following we set $\eta = 0.263 \pm 0.053$ for fermion warm dark matter with zero, or negative, chemical potential, or $\eta = 0.412 \pm 0.082$ for bosons with zero chemical potential. $v_{h\text{rms}}(1)$ is the adiabatic invariant defined in References [4] or [5]. Comparisons with alternative calculations of the free-streaming cut-off wavenumber k_{fs} are presented in **Appendix A**.

4. The Galaxy Generator in Fourier Space

We make use of the galaxy generator described in References [6] and [7]. This program generates galaxies, directly at any given redshift z, given the power spectrum of linear density perturbations $P(k)$. The hierarchical generation of galaxies is illustrated in **Figure 1**. We do not step particles forward in time, but rather work directly in Fourier space at a given redshift z, *i.e.* we generate galaxies in bins of the comoving wavenumber $k_I = 2\pi I/L$ for $I = 2, 3, \cdots, I_{\max}$, with $I_{\max} = 69$.

At each "generation" I, starting at $I = 2$, we calculate the relative density $\delta(\mathbf{x}) \equiv \delta\rho(\mathbf{x})/\langle\rho\rangle$ in the linear approximation by summing its Fourier components up to wavenumber k_I. We then search maximums of $\delta(\mathbf{x})$. If a maximum reaches (or exceeds) 1.69 in the linear approximation, which has already broken down, the *exact* solution (for spherically symmetric density perturbations) diverges, and we generate a galaxy if it "fits". A galaxy i fits if its distance

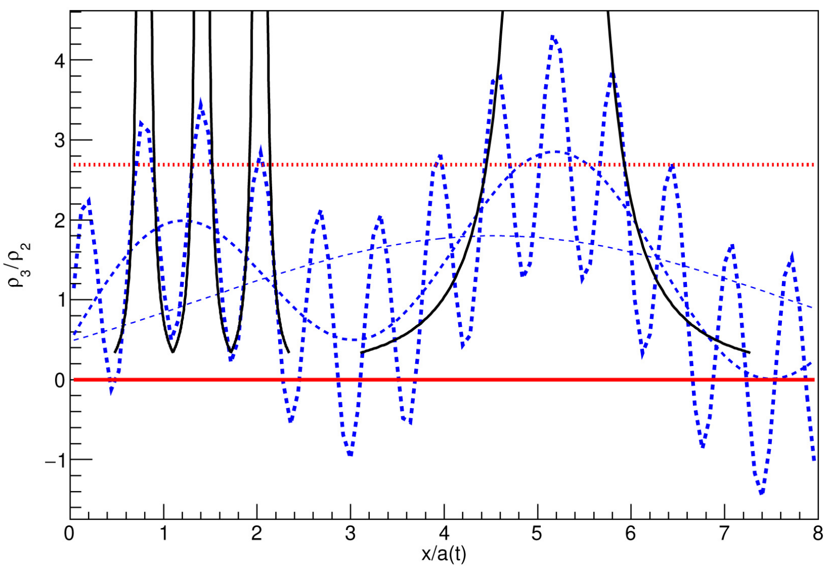

Figure 1. This figure, taken from References [6] or [7], illustrates the hierarchical formation of galaxies. Three Fourier components of the relative density $\delta(\mathbf{x}) \equiv \delta\rho(\mathbf{x})/\langle\rho\rangle$ in the linear approximation are shown. Note that in the linear approximation $\delta(\mathbf{x}) \propto a \propto t^{2/3}$. When $\delta(\mathbf{x})$ reaches 1.69 in the linear approximation, the exact solution diverges and a galaxy forms. As time goes on, density perturbations grow, and groups of galaxies of one generation coalesce into larger galaxies of a new generation as shown on the right.

to all generated galaxies j exceeds $r_j + 0.9r_i$, where $r_i = \pi/k_i$ and $r_j = \pi/k_j$ are their radii [7] (the factor 0.9 was chosen to help "fill" space). After generating all galaxies of generation I, we step $I \to I+1$, and generate the galaxies of generation $I+1$. Note that at generation $I+1$, corresponding to smaller galaxies, a "failed" galaxy that did not "fit" in a generation $\leq I$, may fit at generation $I+1$, and a galaxy is formed that has lost part of its mass to neighboring larger galaxies.

We find it convenient to distinguish two populations of galaxies at every redshift z: the *hierarchical galaxies* that fit, and the *stripped down galaxies* that did not fit, and were generated with a reduced radii. Note that *stripped down galaxies* have lost part of their mass to neighboring larger galaxies, they form near larger galaxies, seldomly in voids, and often are distributed in "filaments" and "sheets". *Hierarchical galaxies* have $M > M_{\text{fs}}$, and *stripped down galaxies* populate all masses, and are the only galaxies with $M < M_{\text{fs}}$ if $\alpha = 0$.

For the cold dark matter ΛCDM model the power spectrum of linear density perturbations is [3]

$$P(k) = \frac{4(2\pi)^3 c^4 N^2 C^2 k \tau^2 \left(\sqrt{2}k/k_{\text{eq}}\right)}{25\Omega_m^2 H_0^4} \left(\frac{k_{\text{SW}}}{k}\right)^{1-n}, \tag{3}$$

with

$$k_{\text{eq}} = \frac{\sqrt{2}H_0(\Omega_m - \Omega_\nu)}{c\sqrt{\Omega_r}}. \tag{4}$$

k is the comoving wavenumber. $\tau\left(\sqrt{2}k/k_{\text{eq}}\right)$ is a function given in Reference [3]. C is a function of Ω_Λ/Ω_m [3]. We take $C = 0.767$ [7]. The amplitude N^2 in (3) is related to $A_s \equiv \Delta_R^2$ [1] by $N^2 \equiv A_s/(4\pi) \equiv \Delta_R^2/(4\pi)$. We take $\ln\left(10^{10}\Delta_R^2\right) = 3.062 \pm 0.029$ [1], corresponding to $N^2 = 1.70\times10^{-10}$. The pivot point is $k_{\text{SW}} = 0.001\ \text{Mpc}^{-1}$. All other cosmological parameters are taken from Reference [1].

For warm dark matter we take the same $P(k)$ for $k < k_{\text{fs}}$. For $k > k_{\text{fs}}$ we replace $P(k)$ by $\alpha P(k)$, where α is a suppression factor. This is the only difference between the simulations for cold and warm dark matter. We use the same seed for the random number generator, so all generated galaxies for $k < k_{\text{fs}}$ are the same for the simulations with cold or warm dark matter. For warm dark matter, the expected value of α, for adiabatic initial conditions, is $\alpha = \left(\Omega_b/\left(\Omega_b + \Omega_c \cdot a_{\text{dec}}/a_{\text{eq}}\right)\right)^2 = 0.0033$. We set $\alpha = 0$ for warm dark matter, but run simulations with several α to understand the onset of damping.

Let us describe the formation of galaxies in time, see **Figure 1**. The relative density $\delta(\mathbf{x})$ is the sum of Fourier components from $I = 2$ up to I_{fs} in the case of warm dark matter (with $\alpha = 0$). Each of these Fourier components grows in proportion to the expansion parameter $a \propto t^{2/3}$. The first galaxies have mass M_{fs}, and form when, at certain locations, the sum of Fourier components of $\delta(\mathbf{x})$ up to $k_{\text{fs}} \equiv I_{\text{fs}} 2\pi/L$ reaches 1.69.

5. Simulations with Redshift z = 0.5

The simulations at redshift $z = 0.5$ are presented in **Table 1**, and in **Figures 2-13**. We note that lowering α from 1 (for the ΛCDM model) to 0 (for the ΛWDM model), reduces the number of galaxies with $M < M_{\text{fs}}$, but the reduction *does not reach zero*. M_{fs} is not a cut-off mass. For warm dark matter, *i.e.* $\alpha = 0$, the reduction factor β is in the range 0.05 to 0.4, depending on the size L, and cut-off wavenumber k_{fs}, of the simulation, and decreases with increasing k. These are *stripped down galaxies*, and their quantitative simulation requires a more complete galaxy generation code, a large simulation size L, and a large dynamic range of galaxy masses. Note how *stripped down galaxies* cluster around the large *hierarchical galaxies*, often forming filament and sheet distributions, and seldom populating the voids. These characteristic features of warm dark matter were noted by P.J.E. Peebles [8].

Table 1. Details of the simulations with redshift $z = 0.5$ presented in **Figures 2-13**. m_h is the mass for fermions with $N_f = 2$, and chemical potential $\mu = 0$, as defined in Section 9.

L	k_{fs}	$\sigma(d_{\text{fs}})$	M_{fs}	$a'_{h\text{NR}}$	$v_{h\text{rms}}(1)$	m_h	Figures
[Mpc]	[Mpc^{-1}]	[Mpc]	$[M_\odot]$		[km/s]	[eV]	
100	2.400	0.654	4.5×10^{10}	0.71×10^{-6}	0.21	205	**2-4**
100	1.200	1.31	3.6×10^{11}	1.58×10^{-6}	0.47	112	**5-7**
500	0.466	3.37	6.1×10^{12}	4.87×10^{-6}	1.46	48	**8-10**
500	0.258	6.09	3.6×10^{13}	10.10×10^{-6}	3.03	28	**11-13**

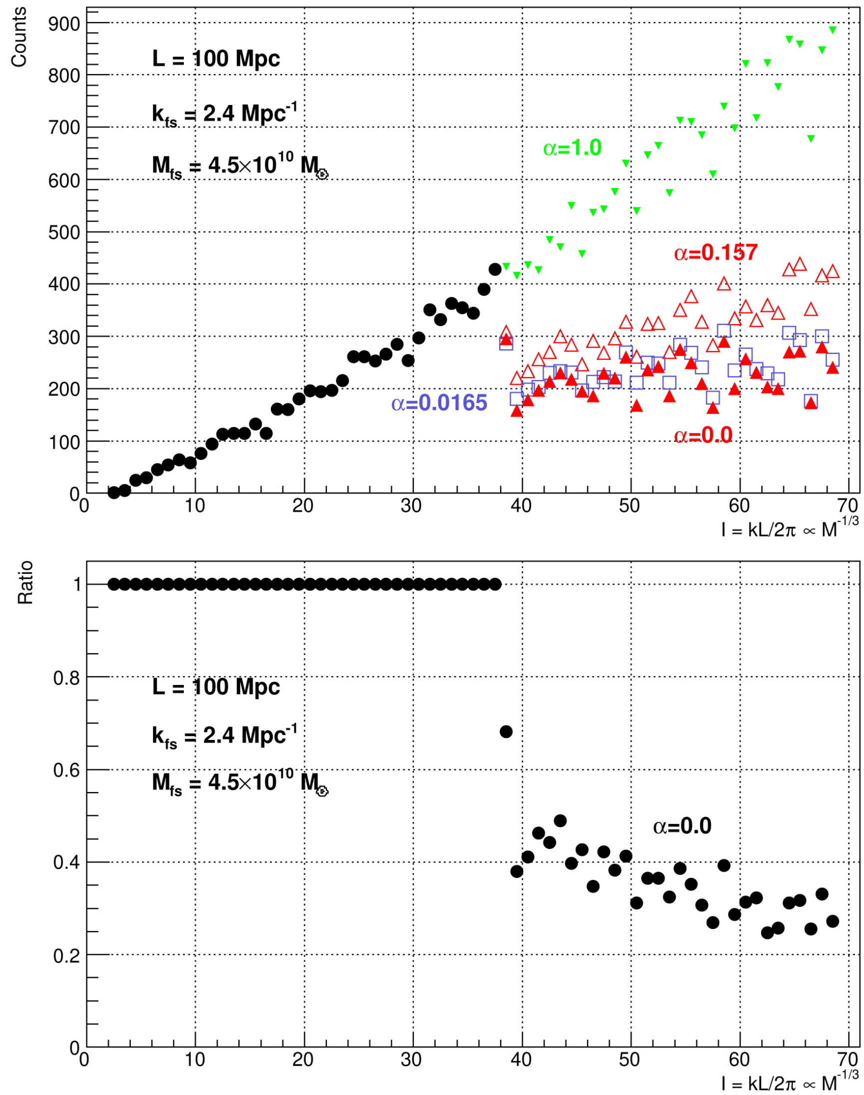

Figure 2. Simulations with $z = 0.5$, $L = 100\ \text{Mpc}$, and $k_{fs} = 2.4\ \text{Mpc}^{-1}$. The corresponding transition galaxy mass is $M_{fs} = 4.5\times10^{10} M_\odot$, and the dark matter particle mass is $m_h = 205\ \text{eV}$ for fermions with $N_f = 2$. Top figure: Distributions of $I = kL/2\pi \propto M^{-1/3}$. Filled circles: distribution of galaxies with $k < k_{fs}$, common to cold and warm dark matter. Shown are distributions of galaxies with $k > k_{fs}$ for $\alpha = 1$ (ΛCDM, inverted green triangles), 0.157, 0.0165, and 0 (ΛWDM, upright red triangles). Bottom figure: Ratio of galaxy counts with $\alpha = 0$ (ΛWDM) and $\alpha = 1$ (ΛCDM). Note that β is in the range 0.4 to 0.3.

6. Comparison with Simulations with Gravitating Particles Stepped Forward in Time

We briefly review a simulation carried out by P. Bode, J. P. Ostriker and N. Turok [9]. Three simulations are done: one ΛCDM simulation, and two ΛWDM simulations with thermal relic dark matter with $m = 350\ \text{eV}$ and 175 eV, respectively, that correspond to a characteristic mass, given by Equation (8) of Reference [9], $M_S = 6.5\times10^{11} M_\odot$ and $7.1\times10^{12} M_\odot$, respectively. M_S corresponds

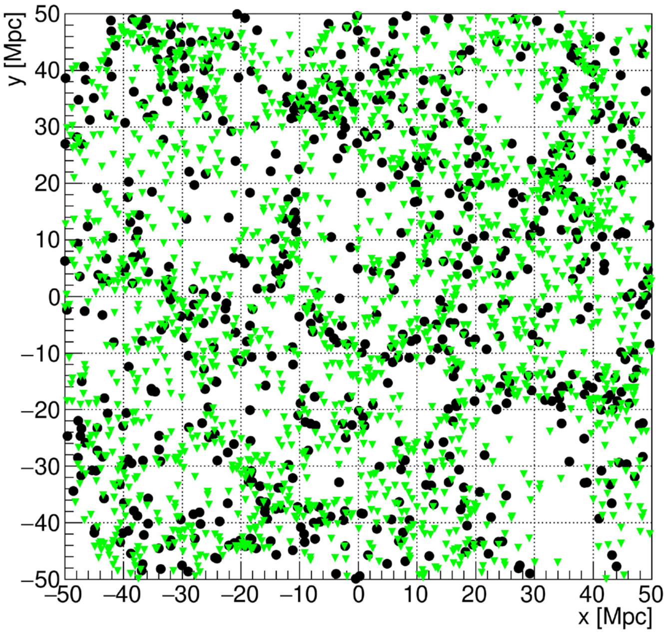

Figure 3. (x, y) distribution of galaxies in a slice of thickness 10 Mpc for the $\alpha = 1$ (ΛCDM) simulation of **Figure 2**. The filled circles are galaxies with $k < k_{fs}$, while triangles are smaller galaxies with $k > k_{fs}$. The simulation has $z = 0.5$, $L = 100$ Mpc, and $k_{fs} = 2.4$ Mpc^{-1}. Smaller and smaller galaxies fill the voids until the wavenumber k reaches the limit k_{max} of the simulation.

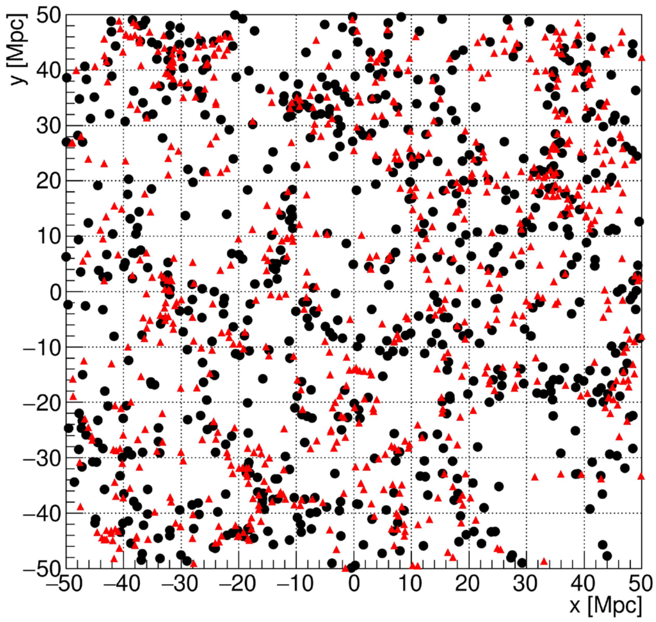

Figure 4. (x, y) distribution of galaxies in a slice of thickness 10 Mpc for the $\alpha = 0$ (ΛWDM) simulation of **Figure 2**. The filled circles are galaxies with $k < k_{fs}$, while triangles are smaller *stripped down galaxies* with $k > k_{fs}$. The simulation has $z = 0.5$, $L = 100$ Mpc, and $k_{fs} = 2.4$ Mpc^{-1}. The *stripped down galaxies* lose mass to neighboring galaxies during their formation, are near larger galaxies, often form filamentary distributions, and seldomly fill voids.

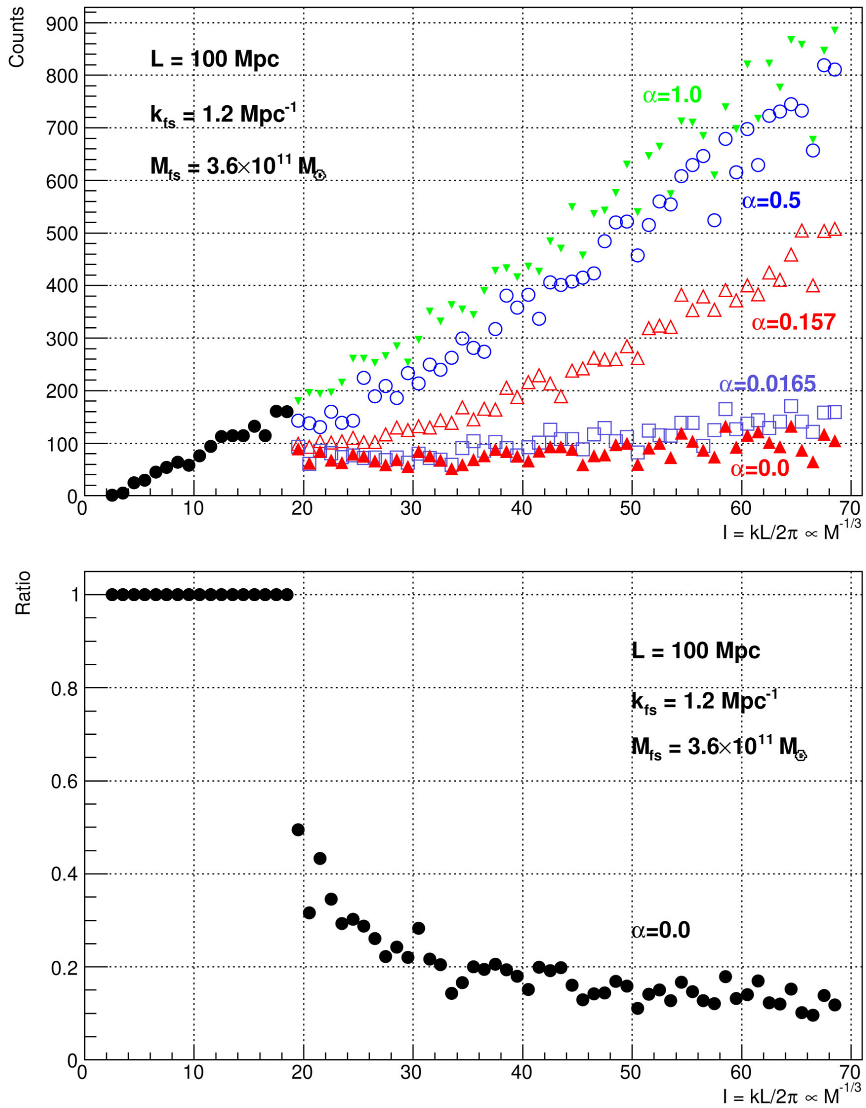

Figure 5. Simulations with $z = 0.5$, $L = 100$ Mpc, and $k_{fs} = 1.2\ \text{Mpc}^{-1}$. The corresponding transition galaxy mass is $M_{fs} = 3.6 \times 10^{11} M_{\odot}$, and the dark matter particle mass is $m_h = 112$ eV for fermions with $N_f = 2$. Top figure: Distributions of $I = kL/2\pi \propto M^{-1/3}$. Filled circles: distribution of galaxies with $k < k_{fs}$, common to cold and warm dark matter. Shown are distributions of galaxies with $k > k_{fs}$ for $\alpha = 1$ (ΛCDM, inverted green triangles), 0.5, 0.157, 0.0165, and 0 (ΛWDM, upright red triangles). Bottom figure: Ratio of galaxy counts with $\alpha = 0$ (ΛWDM) and $\alpha = 1$ (ΛCDM). Note that β is in the range 0.3 to 0.15.

to the total mass of the simulation particles in the collapsed object. The simulations are done in a cube of side 30 Mpc, with 256^3 particles, they resolve objects down to mass $1.5 \times 10^9 M_{\odot}$, and the simulations are carried forward in time up to redshift 1 (limited by computing resources). The authors note that above (below) the characteristic mass scale, the galaxy formation is "bottom up" ("top down"). We quote from the conclusions of Reference [9]: "Below this mass scale (M_S), objects are formed primarily by the fragmentation of pancakes and ribbons.

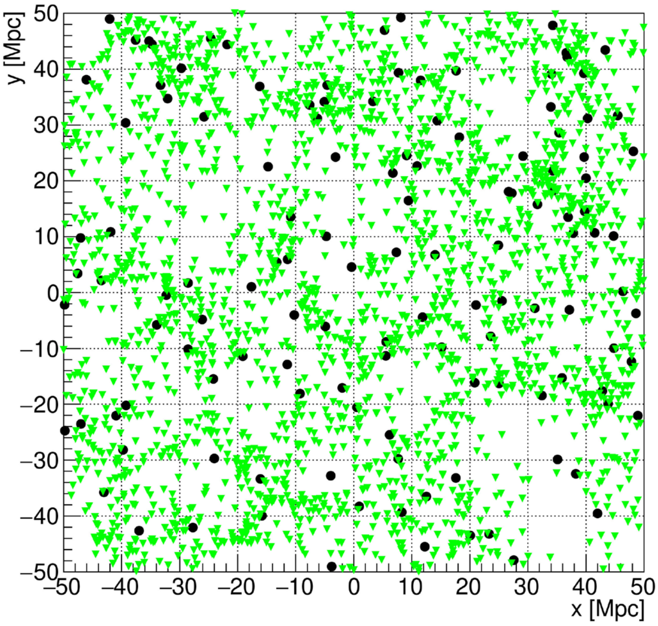

Figure 6. (x, y) distribution of galaxies in a slice of thickness 10 Mpc for the $\alpha = 1$ (ΛCDM) simulation of **Figure 5**. The filled circles are galaxies with $k < k_{fs}$, while triangles are smaller galaxies with $k > k_{fs}$. The simulation has $z = 0.5$, $L = 100$ Mpc, and $k_{fs} = 1.2\ \text{Mpc}^{-1}$. Smaller and smaller galaxies fill the voids until the wavenumber k reaches the limit k_{max} of the simulation.

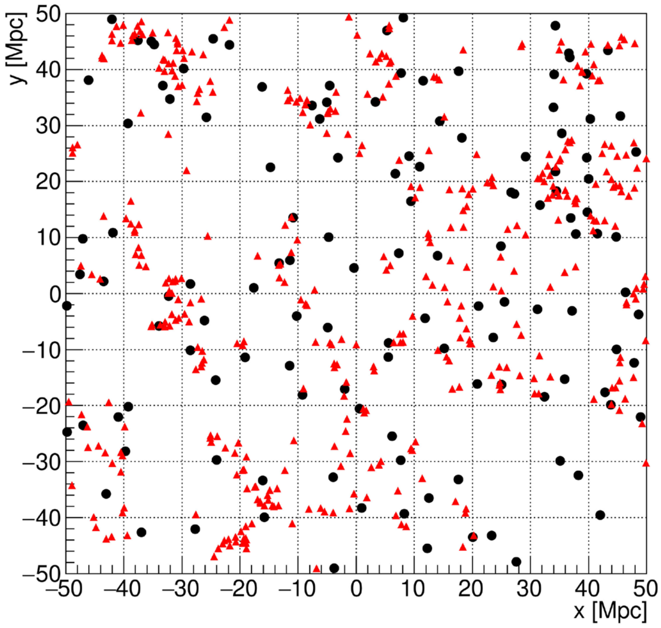

Figure 7. (x, y) distribution of galaxies in a slice of thickness 10 Mpc for the $\alpha = 0$ (ΛWDM) simulation of **Figure 5**. The filled circles are galaxies with $k < k_{fs}$, while triangles are smaller *stripped down galaxies* with $k > k_{fs}$. The simulation has $z = 0.5$, $L = 100$ Mpc, and $k_{fs} = 1.2\ \text{Mpc}^{-1}$. The *stripped down galaxies* lose mass to neighboring galaxies during their formation, are near larger galaxies, often form filamentary distributions, and seldomly fill voids.

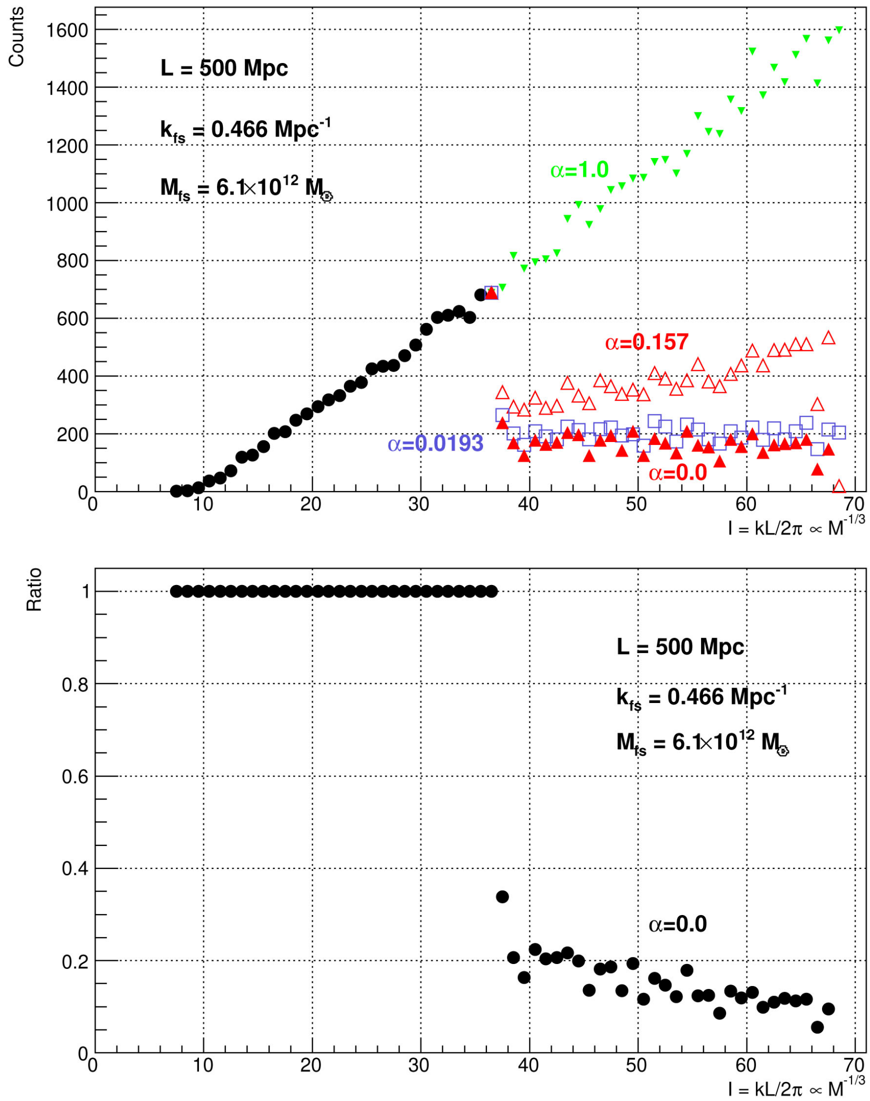

Figure 8. Simulations with $z = 0.5$, $L = 500\,\text{Mpc}$, and $k_{\text{fs}} = 0.466\,\text{Mpc}^{-1}$. The corresponding transition galaxy mass is $M_{\text{fs}} = 6.1 \times 10^{12} M_\odot$, and the dark matter particle mass is $m_h = 48\,\text{eV}$ for fermions with $N_f = 2$. Top figure: Distributions of $I = kL/2\pi \propto M^{-1/3}$. Filled circles: distribution of galaxies with $k < k_{\text{fs}}$, common to cold and warm dark matter. Shown are distributions of galaxies with $k > k_{\text{fs}}$ for $\alpha = 1$ (ΛCDM, inverted green triangles), 0.157, 0.0193, and 0 (ΛWDM, upright red triangles). Bottom figure: Ratio of galaxy counts with $\alpha = 0$ (ΛWDM) and $\alpha = 1$ (ΛCDM). Note that β is in the range 0.2 to 0.05.

They are rarer and considerably less dense than halos of the same mass in ΛCDM. And their spatial distribution is very different—they are concentrated in sheets and ribbons running between the massive halos, an effect which has been noted for some time for dwarf galaxies in the local universe" [8]. "Likewise the apparent absence of dwarf systems in the voids noted by Peebles ..." [8]. With respect to the ΛCDM simulation, the number of halos with mass of order $10^{10} M_\odot$ is reduced by a factor $\beta \approx 0.14$ (0.06) for the $m = 350\,\text{eV}$ (175 eV)

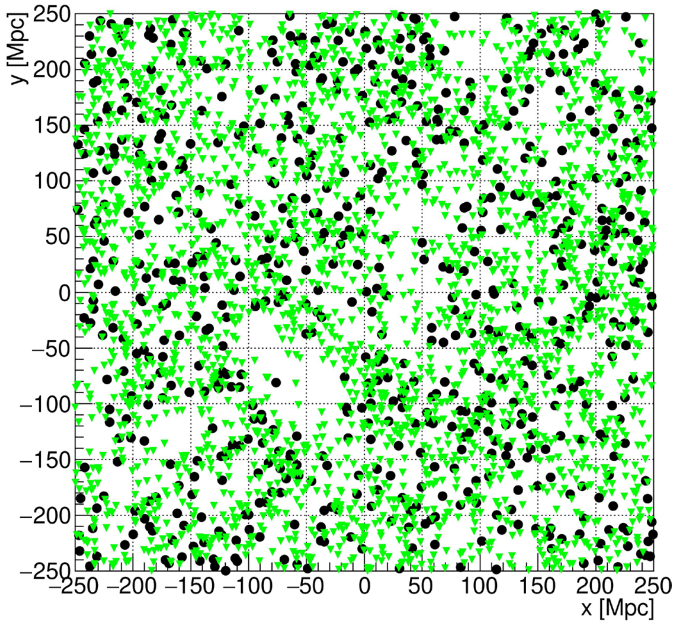

Figure 9. (x, y) distribution of galaxies in a slice of thickness 40 Mpc for the $\alpha = 1$ (ΛCDM) simulation of **Figure 8**. The filled circles are galaxies with $k < k_{fs}$, while triangles are smaller galaxies with $k > k_{fs}$. The simulation has $z = 0.5$, $L = 500$ Mpc, and $k_{fs} = 0.466$ Mpc^{-1}. Smaller and smaller galaxies fill the voids until the wavenumber k reaches the limit k_{max} of the simulation.

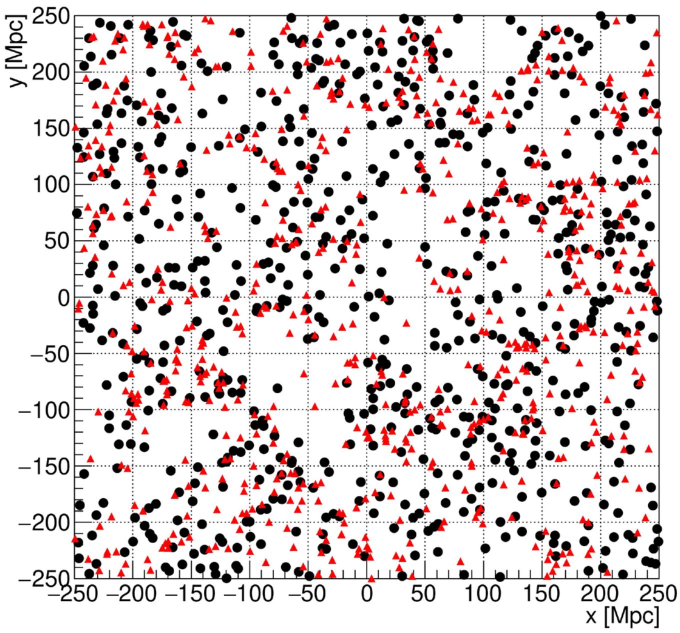

Figure 10. (x, y) distribution of galaxies in a slice of thickness 40 Mpc for the $\alpha = 0$ (ΛWDM) simulation of **Figure 8**. The filled circles are galaxies with $k < k_{fs}$, while triangles are smaller *stripped down galaxies* with $k > k_{fs}$. The simulation has $z = 0.5$, $L = 500$ Mpc, and $k_{fs} = 0.466$ Mpc^{-1}. The *stripped down galaxies* lose mass to neighboring galaxies during their formation, are near larger galaxies, often form filamentary distributions, and seldomly fill voids.

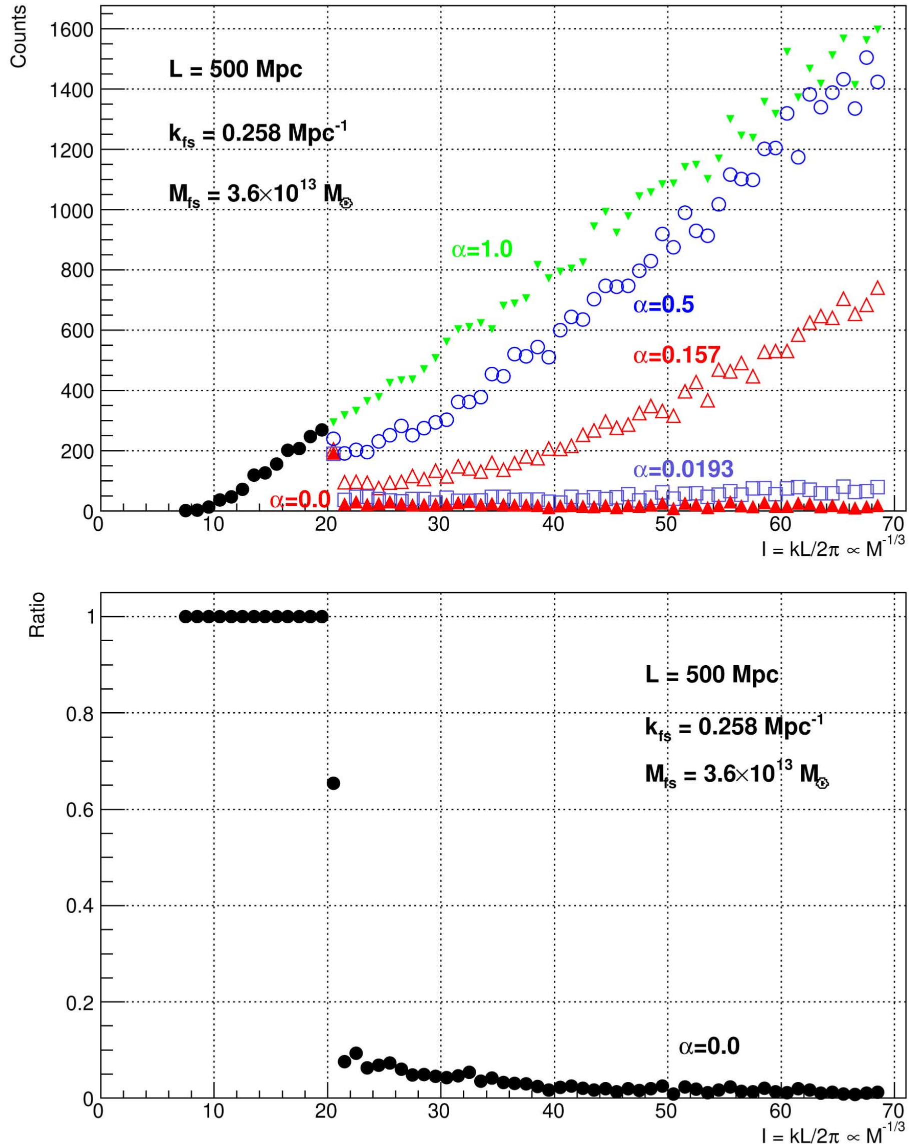

Figure 11. Simulations with $z = 0.5$, $L = 500\,\text{Mpc}$, and $k_{\text{fs}} = 0.258\,\text{Mpc}^{-1}$. The corresponding transition galaxy mass is $M_{\text{fs}} = 3.6 \times 10^{13} M_\odot$, and the dark matter particle mass is $m_h = 28\,\text{eV}$ for fermions with $N_f = 2$. Top figure: Distributions of $I = kL/2\pi \propto M^{-1/3}$. Filled circles: distribution of galaxies with $k < k_{\text{fs}}$, common to cold and warm dark matter. Shown are distributions of galaxies with $k > k_{\text{fs}}$ for $\alpha = 1$ (ΛCDM, inverted green triangles), 0.5, 0.157, 0.0193, and 0 (ΛWDM, upright red triangles). Bottom figure: Ratio of galaxy counts with $\alpha = 0$ (ΛWDM) and $\alpha = 1$ (ΛCDM). Note that β is in the range 0.08 to 0.01.

ΛWDM simulation, at redshift $z = 1$. β increases by a factor 10 from $z = 4$ to $z = 1$ for $m = 350\,\text{eV}$, so the β's for $z = 0.5$ are expected to be larger than for $z = 1$. With respect to the ΛCDM model, the ΛWDM simulations have respectively about 1/5 or 1/9 the number of satellites for a parent of Milky Way mass.

We note that these results are in agreement with our conclusions.

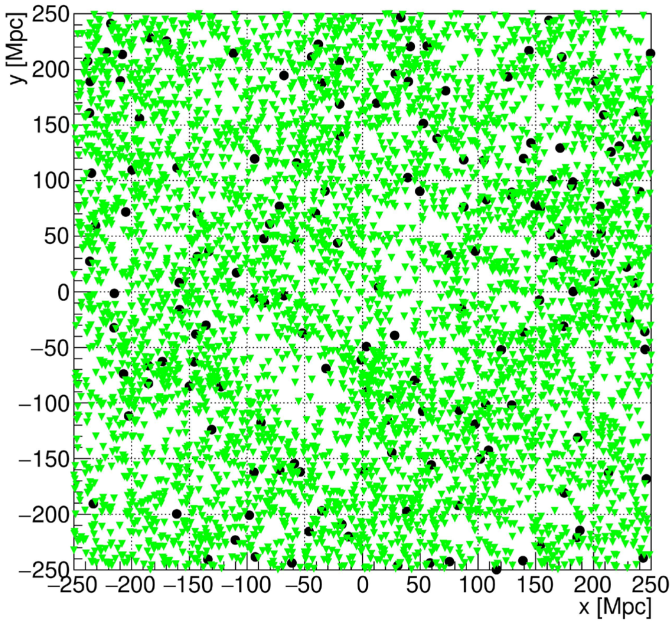

Figure 12. (x, y) distribution of galaxies in a slice of thickness 60 Mpc for the $\alpha = 1$ (ΛCDM) simulation of **Figure 11**. The filled circles are galaxies with $k < k_{fs}$, while triangles are smaller galaxies with $k > k_{fs}$. The simulation has $z = 0.5$, $L = 500$ Mpc, and $k_{fs} = 0.258$ Mpc^{-1}. Smaller and smaller galaxies fill the voids until the wavenumber k reaches the limit k_{max} of the simulation.

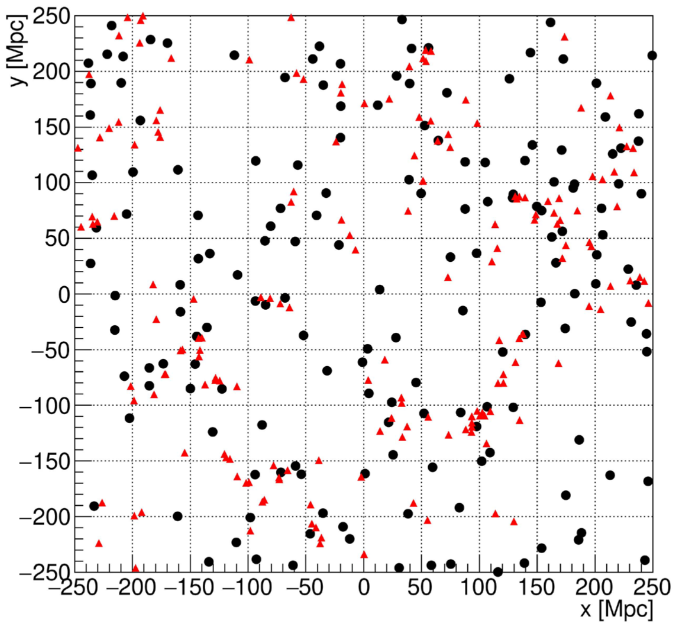

Figure 13. (x, y) distribution of galaxies in a slice of thickness 60 Mpc for the $\alpha = 0$ (ΛWDM) simulation of **Figure 11**. The filled circles are galaxies with $k < k_{fs}$, while triangles are smaller *stripped down galaxies* with $k > k_{fs}$. The simulation has $z = 0.5$, $L = 500$ Mpc, and $k_{fs} = 0.258$ Mpc^{-1}. The *stripped down galaxies* lose mass to neighboring galaxies during their formation, are near larger galaxies, often form filamentary distributions, and seldomly fill voids.

7. Estimate of k_{fs} with the Redshift of First Galaxies

In the warm dark matter scenario, the first galaxies to form have mass M_{fs}. For a larger "smoothing length" π/k_{fs}, M_{fs} increases, and the first galaxies form at a later time, *i.e.* at smaller redshift z_{first}. Therefore, the redshift of the first few galaxies, or the redshift of re-ionization, allows a measurement of k_{fs}. The galaxy with highest spectroscopically confirmed redshift, called GN-z11, has $z = 11.09$. The quasar with highest spectroscopically confirmed redshift has $z = 6.6$. The redshift of re-ionization is $z_{reion} = 8.8^{+1.7}_{-1.4}$ [1]. We will take the redshift of formation of the first (few) galaxies to be $z_{first} = 9.5 \pm 2.0$ (the redshift of the oldest galaxy is statistically uncertain, so in the simulations we extrapolate from galaxies with larger k down to zero counts).

The maximum of the power spectrum of linear density perturbations $P(k)$ is approximately at $k_{eq} = 0.0103\ \text{Mpc}^{-1}$, corresponding to a comoving wavelength $\lambda_{eq} \equiv 2\pi/k_{eq} = 609\ \text{Mpc}$. Therefore, simulations with very large L are required to include the contributions to the relative density perturbation $\delta(\mathbf{x})$ of Fourier components of long wavelength. Such large simulations become prohibitive, so some extrapolation becomes necessary. Simulations corresponding to several redshifts are presented in **Figure 14**. Extrapolating to zero counts we obtain data points in **Figure 15**. From z_{first}, and extrapolating from **Figure 15** we estimate $k_{fs} = 1.1 \pm 0.4\ \text{Mpc}^{-1}$, corresponding to $\log_{10}(M_{fs}/M_\odot) = 11.67 \pm 0.50$.

8. Measurement of M_{fs} with Galaxy Mass Distributions

Figure 16 and **Figure 17** present distributions of galaxy stellar masses. The data is from the Sloan Digital Sky Survey SDSS DR15 [10]. The simulations help us identify the peak marked "M_{sfs}" corresponding to the cut-off wavenumber k_{fs}. We obtain the transition stellar mass $\log_{10}(M_{fs}/M_\odot) = 11.63 \pm 0.15 \pm 0.13$ (the latter uncertainty is an upper bound to the SDSS measurement uncertainty). Note that first galaxies, *i.e.* galaxies with old stellar populations, have a mass approximately equal to M_{sfs}, which is an alternative way to identify "M_{sfs}".

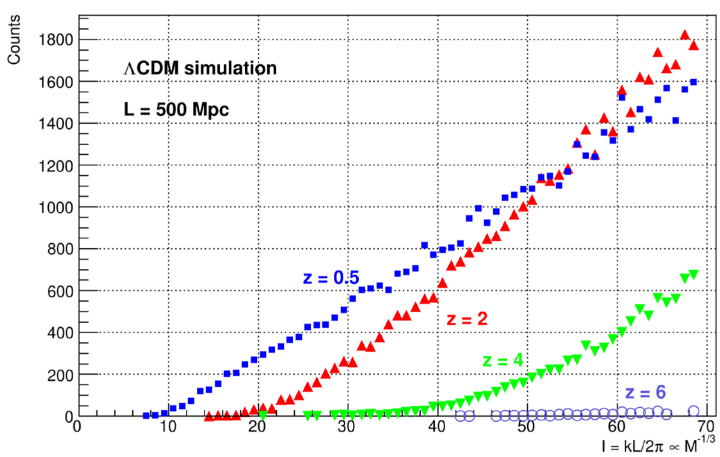

Figure 14. Distributions of $I = kL/2\pi \propto M^{-1/3}$ for simulations with $L = 500\ \text{Mpc}$, and redshifts $z = 0.5$, $z = 2$, $z = 4$, and $z = 6$ in the ΛCDM scenario.

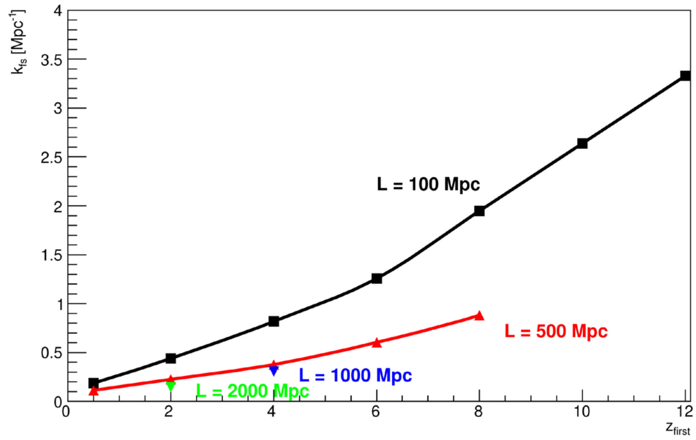

Figure 15. Shown are the cut-off wavenumbers k_{fs} of the first (few) galaxies obtained from simulations with $L = 100$, 500, 1000, or 2000 Mpc, and the indicated redshift z_{first}. The points corresponding to $z_{first} = 0.5$ are obtained from Figure 2 or Figure 5 for $L = 100$ Mpc, and Figure 8 or Figure 11 for $L = 500$ Mpc, by extrapolation to zero counts. Points corresponding to $L = 500$ Mpc are obtained from Figure 14, by extrapolation to zero counts. Note that k_{fs} requires simulations with $L \gtrsim 500$ Mpc.

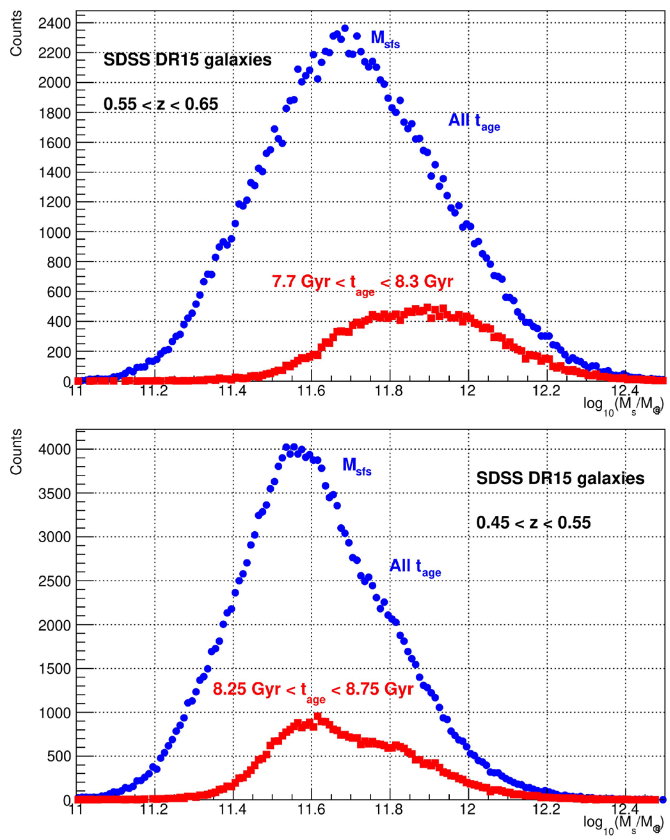

Figure 16. Distribution of $\log_{10}(M_s/M_\odot)$ for all galaxy stellar ages t_{age}, and for old stellar ages, for 0.55 < z < 0.65 (top figure), and 0.45 < z < 0.55 (bottom figure). M_s is the stellar mass of the galaxies. We obtain $\log_{10}(M_{sfs}/M_\odot) \approx 11.68$, and $\log_{10}(M_{sfs}/M_\odot) \approx 11.57$, respectively.

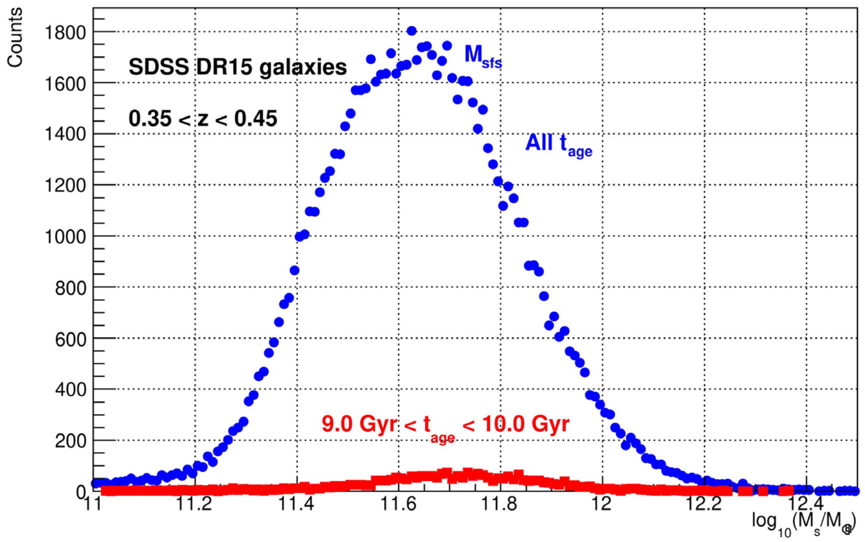

Figure 17. Distribution of $\log_{10}\left(M_s/M_\odot\right)$ for all galaxy stellar ages t_{age}, and for the galaxies with $9\ \text{Gyr} < t_{\text{age}} < 10\ \text{Gyr}$, for $0.35 < z < 0.45$. We obtain $\log_{10}\left(M_{sfs}/M_\odot\right) \approx 11.63$.

To the stellar mass M_{sfs} we need to add the mass of gas to obtain the mass of baryons M_{bfs}, and then add the dark matter mass to obtain M_{fs}. To make these transitions using data, we select a large relaxed spiral galaxy in the SPARC sample [11], *i.e.* UGC11914. The observed circular velocity of rotation at the last observed radius ($r = 9.83$ kpc) is 305.00 ± 5.07 km/s. The corresponding velocity contributions from gas, stars in the disk, and stars in the bulge, are 29.29 km/s, 121.61 km/s, and 82.73 km/s, respectively (taking the stellar mass-to-light ratios to be $0.3M_\odot/L_\odot$ for the disk, and $1.4 \cdot 0.3M_\odot/L_\odot$ for the bulge [5] [11]). These velocities contribute in quadrature. We obtain $\log_{10}\left(M_{bfs}/M_\odot\right) = 11.65 \pm 0.20$, and $\log_{10}\left(M_{\text{fs}}/M_\odot\right) = 12.26 \pm 0.28$. (An alternative determination of M_{fs}, is to multiply M_{bfs} by $\left(\Omega_b + \Omega_c\right)/\Omega_b$, that obtains $\log_{10}\left(M_{\text{fs}}/M_\odot\right) = 12.45$.)

Note, in Figure 17, the distribution of *stripped down galaxies* for $M_s < M_{sfs}$.

9. Measurement of $v_{h\text{rms}}(1)$ with Spiral Galaxy Rotation Curves

The root-mean-square (rms) velocity of non-relativistic dark matter particles in the early universe, when density perturbations are relatively small, can be written in the form

$$v_{h\text{rms}}(a) = \frac{v_{h\text{rms}}(1)}{a}, \tag{5}$$

where a is the expansion parameter. Equation (5) assumes that dark matter decouples from the Standard Model sector, and from self-annihilation, while density perturbations are still relatively small. However, dark matter-dark matter elastic scattering is allowed. The "adiabatic invariant" $v_{h\text{rms}}(1)$ has been measured [5] by fitting 40 spiral galaxy rotation curves in the SPARC sample [11]. We take

$$v_{hrms}(1) = (0.82 \pm 0.31)\sqrt{1-\kappa_h} \text{ km/s} = 0.76 \pm 0.29 \text{ km/s}. \tag{6}$$

The factor $\sqrt{1-\kappa_h}$ is a correction for possible dark matter rotation. We take $\kappa = 0.15 \pm 0.15$ [4] [5] [12]. Equation (6) is consistent with **Figure 4** of Reference [5] for non-degenerate dark matter, and with **Figure 7** for fermion dark matter with chemical potential $\mu \approx 0$. This range is also consistent with 10 galaxies in the THINGS sample [5] [13]. (The different normalizations used for baryons in our analysis of the SPARC and THINGS samples is discussed in Reference [5], and accounts for the difference of m_h between the measurement in Reference [4] and the present result.) The expansion parameter at which the dark matter becomes non-relativistic is defined as

$$a'_{h\mathrm{NR}} \equiv \frac{v_{hrms}(1)}{c} = (2.54 \pm 0.97) \times 10^{-6}, \tag{7}$$

(not to be confused with $a_{h\mathrm{NR}}$ in **Appendix A**). Note that $a'_{h\mathrm{NR}}$ is less than the expansion parameter at matter-radiation equality, $a_{\mathrm{eq}} = (2.97 \pm 0.04) \times 10^{-4}$, *i.e.* we are dealing with warm dark matter. This $a'_{h\mathrm{NR}}$ corresponds to $\sigma(d_{\mathrm{fs}}) = 1.96 \pm 0.63 \pm 0.40$ Mpc (the second uncertainty is due to the uncertainty of η), $k_{\mathrm{fs}} = 0.80^{+0.42}_{-0.24}$ Mpc^{-1}, and $\log_{10}(M_{\mathrm{fs}}/M_\odot) = 12.08 \pm 0.50$ for fermion dark matter; or $\sigma(d_{\mathrm{fs}}) = 3.07 \pm 0.54 \pm 0.61$ Mpc, $k_{\mathrm{fs}} = 0.51^{+0.28}_{-0.15}$ Mpc^{-1}, and $\log_{10}(M_{\mathrm{fs}}/M_\odot) = 12.66 \pm 0.50$ for boson dark matter.

The adiabatic invariant $v_{hrms}(1)$ determines the ratio of dark matter temperature-to-mass $T_h(a)/m_h$, so one more constraint is needed to obtain $T_h(a)$ and m_h separately. It turns out that, if we assume that dark matter has zero chemical potential, and decouples (from the Standard Model sector, and from self-annihilation) while still ultra-relativistic, then dark matter is also in thermal equilibrium with the Standard Model sector in the early universe *for the measured values of* $v_{hrms}(1)$ and T_0 [4] [12]!

10. Dark Matter with Zero Chemical Potential

Dark matter with chemical potential $\mu = 0$ is special. It corresponds to dark matter that was once in diffusive equilibrium with the Standard Model sector and decoupled (from the Standard Model sector, and from self-annihilation) while still ultra-relativistic, and/or dark matter composed of equal number densities of fermions and anti-fermions, or may be the case in scenarios with sterile Majorana neutrinos, or bosons.

The mass of dark matter particles with $\mu = 0$, and with the observed mean dark matter density of the universe $\Omega_c \rho_{\mathrm{crit}}$, is presented in Equation (18) of **Appendix B**. For fermions with chemical potential $\mu = 0$,

$$m_h = 78.5 \left(\frac{0.76 \text{ km/s}}{v_{hrms}(1)} \right)^{3/4} \left(\frac{2}{N_f} \right)^{1/4} \text{eV}. \tag{8}$$

For bosons with chemical potential $\mu = 0$,

$$m_h = 51.1\left(\frac{0.76\ \text{km/s}}{v_{h\text{rms}}(1)}\right)^{3/4}\left(\frac{1}{N_b}\right)^{1/4}\ \text{eV}. \tag{9}$$

If dark matter decouples from the Standard Model sector, and from self-annihilation, while ultra-relativistic, the ratio of dark matter-to-photon temperatures after e^+e^- annihilation, while dark matter is still ultra-relativistic, is [4]

$$\frac{T_h}{T} = 0.373\left(\frac{v_{h\text{rms}}(1)}{0.76\ \text{km/s}}\right)^{1/4}\left(\frac{2}{N_f}\right)^{1/4} \tag{10}$$

for fermions with $\mu = 0$, and

$$\frac{T_h}{T} = 0.492\left(\frac{v_{h\text{rms}}(1)}{0.76\ \text{km/s}}\right)^{1/4}\left(\frac{1}{N_b}\right)^{1/4} \tag{11}$$

for bosons with $\mu = 0$. The temperature ratio (10) corresponds to dark matter with $N_f = 2$ decoupling from the Standard Model sector, and from self-annihilation, while still ultra-relativistic, in the approximate temperature range from m_c to m_b [12]. Note that assuming $\mu = 0$ obtains thermal equilibrium *with the measured values of* $v_{h\text{rms}}(1)$ and T_0! Is this a coincidence? This result is consistent with Big Bang Nucleosynthesis [12].

11. Thermal Relic

Let us now consider dark matter that was in *both diffusive and thermal equilibrium* with the Standard Model sector. Diffusive equilibrium implies chemical potential $\mu = 0$. The *thermal relic* mass for warm dark matter with $\mu = 0$, that decouples from the Standard Model sector, and from self-annihilation, while still ultra-relativistic, is [1]

$$m_{\text{th}} = \frac{112.7\ \text{eV}}{N_b + 3N_f/4}\left(\frac{0.378}{T_h/T}\right)^3, \tag{12}$$

where N_f (N_b) is the number of fermion (boson) degrees of freedom, and T_h/T is the ratio of dark matter-to-photon temperatures after e^+e^- annihilation while dark matter is still ultra-relativistic. $T_h/T = 0.378$ if dark matter decouples from the Standard Model sector, and from self-annihilation, in the temperature range from m_c to m_τ. T_h/T ranges from 0.344 for decoupling in the temperature range m_H to m_t, to, say, 0.424 for decoupling in the temperature range T_c to m_s [12]. Setting $m_{\text{th}} = m_h$, for the case $\mu = 0$, and allowing T_h/T to be in the range 0.424 to 0.344, obtains a measurement of $v_{h\text{rms}}(1)$ that is *independent of spiral galaxy rotation curves*.

A summary of the four independent measurements is presented in **Table 2** for both fermions and bosons. Note that setting $m_{\text{th}} = m_h$, and assuming that T_h/T is in the range from 0.344 to 0.424, obtains $v_{h\text{rms}}(1)$ in agreement with three independent measurements in **Table 2**. This agreement is either a coincidence,

Table 2. Summary of four independent measurements of the adiabatic invariant $v_{h\text{rms}}(1)$, the expansion parameter at which dark matter particles become non-relativistic $a'_{h\text{NR}}$, the cut-off wavenumber of warm dark matter k_{fs}, the transition galaxy mass M_{fs}, and the mass m_h of dark matter particles (for the case of zero chemical potential, see discussion in Section 11). The top (bottom) Table is for fermions with $N_f = 2$ and $\eta = 0.263 \pm 0.053$ (bosons with $N_b = 1$ and $\eta = 0.412 \pm 0.082$). *For this row we take the dark matter-to-photon temperature T_h/T, after e^+e^- annihilation, while dark matter is still ultra-relativistic, to be 0.378 (with limits 0.344 to 0.424 [12]).

Fermions	$v_{h\text{rms}}(1)$	$a'_{h\text{NR}} \times 10^6$	m_h	k_{fs}	$\log_{10}(M_{\text{fs}}/M_\odot)$
Observable	[km/s]		[eV]	[Mpc^{-1}]	
Spiral galaxies	0.76 ± 0.29	2.54 ± 0.97	79^{+35}_{-17}	$0.80^{+0.42}_{-0.24}$	12.08 ± 0.50
$m_{\text{th}} = m_h$ *	$0.81^{+0.47}_{-0.25}$	$2.69^{+1.57}_{-0.84}$	75 ± 23	0.76 ± 0.31	12.14 ± 0.52
First galaxies	$0.52^{+0.38}_{-0.19}$	$1.75^{+1.29}_{-0.63}$	104 ± 38	1.10 ± 0.40	11.67 ± 0.50
M_{fs} from SDSS	$0.90^{+0.32}_{-0.26}$	$3.00^{+1.07}_{-0.89}$	69 ± 18	0.70 ± 0.15	12.26 ± 0.28
Bosons	$v_{h\text{rms}}(1)$	$a'_{h\text{NR}} \times 10^6$	m_h	k_{fs}	$\log_{10}(M_{\text{fs}}/M_\odot)$
Observable	[km/s]		[eV]	[Mpc^{-1}]	
Spiral galaxies	0.76 ± 0.29	2.54 ± 0.97	51^{+22}_{-11}	$0.51^{+0.28}_{-0.15}$	12.66 ± 0.50
$m_{\text{th}} = m_h$ *	$0.26^{+0.16}_{-0.08}$	$0.88^{+0.52}_{-0.28}$	113 ± 35	1.26 ± 0.50	11.49 ± 0.52
First galaxies	$0.31^{+0.23}_{-0.11}$	$1.04^{+0.74}_{-0.38}$	100 ± 39	1.10 ± 0.40	11.67 ± 0.50
M_{fs} from SDSS	$0.53^{+0.18}_{-0.16}$	$1.77^{+0.61}_{-0.52}$	67 ± 18	0.70 ± 0.17	12.26 ± 0.28

or is evidence that indeed $\mu/(kT_h) \approx 0$, and dark matter was in both diffusive and thermal equilibrium with the Standard Model sector in the early universe (within uncertainties), and decoupled from the Standard Model sector, and from self-annihilation, while still ultra-relativistic; and, furthermore, that the mass of dark matter particles is indeed given by Equation (8) for fermions, or (9) for bosons.

The case of negative μ/kT_h, with large $m_h c^2 \approx kT_h(a_{h\text{NR}})$, with the same measured $a_{h\text{NR}}$ and $v_{h\text{rms}}(1)$, can not be ruled out, but is not compelling: it requires a *coincidence* of $m_{\text{th}} = m_h$ with the measured $v_{h\text{rms}}(1)$ and T_0, implies that dark matter was never in thermal or diffusive equilibrium with the Standard Model sector, yet requires self-annihilation and freeze-out to obtain the observed dark matter density.

12. Conclusions

To understand warm dark matter, we find it convenient to classify galaxies, at any given redshift z, according to their origin: *hierarchical galaxies*, and *stripped down galaxies*. *Hierarchical galaxies* form from the bottom up: the first galaxies to form, in the warm dark matter scenario, have mass M_{fs}, these galaxies cluster due to gravity, coalesce, and form galaxies of a new generation, in an ongoing hierarchical formation of galaxies, as illustrated in Figure 1. During their formation, *stripped down galaxies* lose part of their mass to neighboring galaxies. *Hie-*

rarchical galaxies have masses $M > M_{\text{fs}}$, and dominate galaxies with $M > M_{\text{fs}}$. *Stripped down galaxies* populate all masses, $M > M_{\text{fs}}$ and $M < M_{\text{fs}}$, and are the only galaxies with $M < M_{\text{fs}}$. The "smoothing length" π/k_{fs} suppresses *Hierarchical galaxies* with $M < M_{\text{fs}}$, but does not smooth the density perturbations of *stripped down galaxies* that are created highly non-linear.

In **Table 2**, we present a summary of four *independent* measurements of k_{fs} and m_h, separately for fermion and boson dark matter. These measurements are based on:

1) Spiral galaxy rotation curves (that obtain $v_{h\text{rms}}(1)$),

2) The assumption that dark matter was once in thermal and diffusive equilibrium with the Standard Model sector, and decoupled while still ultra-relativistic: measures $m_{\text{th}} = m_h$, and $v_{h\text{rms}}(1)$, (this analysis has no input from spiral galaxy rotation curves),

3) The redshift of formation of first galaxies (measures k_{fs}), and

4) The distributions of masses of SDSS galaxies (measures M_{fs}).

The conclusions of these studies are:

- By construction, the generated galaxies are exactly the same for cold and warm dark matter for $M > M_{\text{fs}}$ (if the same random number seed is used), so all successes of the ΛCDM model are preserved.
- For warm dark matter, the distribution of galaxy masses becomes suppressed for $M < M_{\text{fs}}$ by a factor β. From the simulations, β is in the approximate range 0.05 to 0.4. The value of β is sensitive to the size L of the simulation and to k_{fs}, and requires a more detailed implementation of the galaxy generator, and hence is uncertain. From data, β can reach approximately 0.68 at $k = 1.2k_{\text{fs}}$, see **Figure 16**.
- The distributions of galaxies with $M < M_{\text{fs}}$ are very different for the cold and warm dark matter scenarios. For warm dark matter there are huge empty voids, the *stripped down galaxies* with $M < M_{\text{fs}}$ cluster near neighboring larger galaxies, and often are distributed in filaments and sheets. These characteristic features of warm dark matter were noted by P. J. E. Peebles [8].
- In **Table 2** we have presented four independent measurements. The first two determine $a'_{h\text{NR}}$ and hence $\sigma(d_{\text{fs}})$, while the last two measurements obtain k_{fs}. The relation $2\sigma(d_{\text{fs}}) = \pi/k_{\text{fs}}$ is well satisfied, so the "smoothing length" π/k_{fs} is indeed due to free-streaming dispersion, and not to diffusion of self interacting dark matter, or to other causes.
- The mass of the Milky Way galaxy is approximately equal to the measured transition mass M_{fs}. The warm dark matter scenario with this M_{fs} solves, at least qualitatively, all problems of the "small scale crisis" mentioned in the Introduction.
- Several analysis of the Lyman-α forest, and of gravitational lensing, of light from distant quasars, have set lower limits on the *thermal relic mass*, typically in the range 2000 eV to 4000 eV. (Such thermal relics are assumed to self-annihilate and freeze out, to obtain the present mean dark matter density of the universe.) These limits are equivalent to setting lower limits on k_{fs} in

the range 10 Mpc^{-1} to 21 Mpc^{-1}, in disagreement with the measurements presented in Table 2. Note that these limits depend on accurate simulations of the hydrogen or dark matter densities of non-linear *stripped down galaxies* at redshift $z \approx 5.4$. These discrepancies between the limits and our measurements of k_{fs} need to be resolved.

- Let us consider fermion dark matter with $N_f = 2$. From the excellent agreement of the four independent measurements presented in Table 2, we conclude that dark matter was once in thermal and diffusive equilibrium with the Standard Model sector, and decoupled (from the Standard Model sector, and from self-annihilation) while still ultra-relativistic, and in the approximate temperature range from m_c to m_b. These dark matter particles have a mass $m_h = 75 \pm 23\ \text{eV}$. The case of Majorana sterile neutrino warm dark matter was illustrated in Figure 11 of Reference [12].

Acknowledgements

The simulations in this article were made possible by the High Power Computing Center of Universidad San Francisco de Quito.

Funding for the Sloan Digital Sky Survey IV has been provided by the Alfred P. Sloan Foundation, the U.S. Department of Energy Office of Science, and the Participating Institutions. SDSS acknowledges support and resources from the Center for High-Performance Computing at the University of Utah. The SDSS web site is www.sdss.org.

SDSS-IV is managed by the Astrophysical Research Consortium for the Participating Institutions of the SDSS Collaboration including the Brazilian Participation Group, the Carnegie Institution for Science, Carnegie Mellon University, the Chilean Participation Group, the French Participation Group, Harvard-Smithsonian Center for Astrophysics, Instituto de Astrofísica de Canarias, The Johns Hopkins University, Kavli Institute for the Physics and Mathematics of the Universe (IPMU)/University of Tokyo, the Korean Participation Group, Lawrence Berkeley National Laboratory, Leibniz Institut für Astrophysik Potsdam (AIP), Max-Planck-Institut für Astronomie (MPIA Heidelberg), Max-Planck-Institut für Astrophysik (MPA Garching), Max-Planck-Institut für Extraterrestrische Physik (MPE), National Astronomical Observatories of China, New Mexico State University, New York University, University of Notre Dame, Observatário Nacional/MCTI, The Ohio State University, Pennsylvania State University, Shanghai Astronomical Observatory, United Kingdom Participation Group, Universidad Nacional Autónoma de México, University of Arizona, University of Colorado Boulder, University of Oxford, University of Portsmouth, University of Utah, University of Virginia, University of Washington, University of Wisconsin, Vanderbilt University, and Yale University.

Conflicts of Interest

The author declares no conflicts of interest regarding the publication of this paper.

References

[1] Tanabashi, M., *et al.*, (Particle Data Group) (2018) The Review of Particle Physics. *Physical Review* D, **98**, Article ID: 030001. https://doi.org/10.1103/PhysRevD.98.030001

[2] Drewes, M., *et al.* (2017) A White Paper on keV Sterile Neutrino Dark Matter. *Journal of Cosmology and Astroparticle Physics*, **2017**, 25. https://doi.org/10.1088/1475-7516/2017/01/025

[3] Weinberg, S. (2008) Cosmology. Oxford University Press, Oxford.

[4] Hoeneisen, B. (2019) A Study of Dark Matter with Spiral Galaxy Rotation Curves. Part II. *International Journal of Astronomy and Astrophysics*, **9**, 133-141. https://doi.org/10.4236/ijaa.2019.92010

[5] Hoeneisen, B. (2019) The Adiabatic Invariant of Dark Matter in Spiral Galaxies. *International Journal of Astronomy and Astrophysics*, **9**, 355-367.

[6] Hoeneisen, B. (2000) A Simple Model of the Hierarchical Formation of Galaxies. arXiv:astro-ph/0009071.

[7] Hoeneisen, B. (2018) Study of Galaxy Distributions with SDSS DR14 Data and Measurement of Neutrino Masses. *International Journal of Astronomy and Astrophysics*, **8**, 230-257. https://doi.org/10.4236/ijaa.2018.83017

[8] Peebles, P.J.E. (2001) The Void Phenomenon. *The Astronomical Journal*, **557**, 495-504. https://doi.org/10.1086/322254

[9] Bode, P., Ostriker, J.P. and Turok, N. (2001) Halo Formation in Warm Dark Matter Models, Astrophys.J., **556**, 93-107. https://doi.org/10.1086/321541

[10] Aguado, D.S., *et al.* (2018) The Fifteenth Data Release of the Sloan Digital Sky Surveys: First Release of MaNGA Derived Quantities, Data Visualization Tools and Stellar Library. arXiv:1812.02759.

[11] Lelli, F., McGaugh, S.S. and Schombert, J.M. (2016) SPARC: Mass Models for 175 Disk Galaxies with *Spitzer* Photometry and Accurate Rotation Curves. *The Astronomical Journal*, **152**, 157. https://doi.org/10.3847/0004-6256/152/6/157

[12] Hoeneisen, B. (2019) A Study of Dark Matter with Spiral Galaxy Rotation Curves. *International Journal of Astronomy and Astrophysics*, **9**, 71-96. https://doi.org/10.4236/ijaa.2019.92007

[13] de Blok, W.J.G., *et al.* (2008) High-Resolution Rotation Curves and Galaxy Mass Models from Things. *The Astronomical Journal*, **136**, 2648-2719. https://doi.org/10.1088/0004-6256/136/6/2648

[14] Viel, M., Becker, G.D., Bolton, J.S. and Haehnelt, M.G. (2013) Warm Dark Matter as a Solution to the Small Scale Crisis: New Constraints from High Redshift Lyman-α Forest Data. *Physical Review D*, **88**, Article ID: 043502. https://doi.org/10.1103/PhysRevD.88.043502

[15] Viel, M., Lesgourgues, J., Haehnelt, M.G., Matarrese, S. and Riotto, A. (2005) Constraining Warm Dark Matter Candidates Including Sterile Neutrinos and Light Gravitinos with WMAP and the Lyman-Forest. *Physical Review D*, **71**, Article ID: 063534. https://doi.org/10.1103/PhysRevD.71.063534

[16] Boyanovsky, D., de Vega, H.J. and Sanchez, N.G. (2008) The Dark Matter Transfer Function: Free Streaming, Particle Statistics and Memory of Gravitational Clustering, *Physical Review D*, **78**, Article ID: 063546. https://doi.org/10.1103/PhysRevD.78.063546

Appendix A. Comments on the Cut-Off Wavenumber k_{fs}

In this article we obtain k_{fs} form $2\sigma(d_{\text{fs}}) = \lambda_{\text{fs}}/2 = \pi/k_{\text{fs}}$ with

$$\sigma(d_{\text{fs}}) = \eta \frac{c a'_{h\text{NR}}}{H_0}\left[\frac{1}{\sqrt{\Omega_r}}\ln\left(2\frac{a_{\text{eq}}}{a'_{h\text{NR}}}\right) + \frac{2}{\sqrt{\Omega_m}}\left(a_{\text{eq}}^{-1/2} - a_{\text{dec}}^{-1/2}\right)\right], \tag{13}$$

with $\eta = 0.2816, 0.2628$, and 0.4115 for negative chemical potential $\mu < 0$, fermions with $\mu = 0$, and bosons with $\mu = 0$, respectively. For an early thermal relic the ratio of dark matter-to-photon temperatures after e^+e^- annihilation, while dark matter is still ultra-relativistic, is $T_h/T = 0.344$. Then, for early thermal relics, $a'_{h\text{NR}} \equiv v_{h\text{rms}}(1)/c = (1.523/0.6694)\cdot 0.344 kT_0/(m_h c^2)$ for fermions, and $a'_{h\text{NR}} = (0.8139/0.7269)\cdot 0.344 kT_0/(m_h c^2)$ for bosons, see **Appendix B**. Note that we extended the integral in (1) to a_{dec}, when baryon acoustic oscillations freeze, and gravity from baryons dominate for $k > k_{\text{fs}}$. In Table B we compare this reference calculation of k_{fs} with several alternatives.

As an alternative to the reference calculation, we could have integrated up to a_{eq}, and obtained

$$\sigma(d_{\text{fs}}) = \eta \frac{c a'_{h\text{NR}}}{H_0\sqrt{\Omega_r}}\ln\left(2\frac{a_{\text{eq}}}{a'_{h\text{NR}}}\right), \tag{14}$$

with $\eta = 0.2707, 0.2518$, and 0.4031 for $\mu < 0$, fermions with $\mu = 0$, and bosons with $\mu = 0$, respectively.

Reference [14] obtains a lower limit of 2500 eV (at 3σ) for the mass of thermal relic dark matter from a study of the Lyman-α forest of distant quasar light. The free-streaming cut-off wavenumber $k_{1/2}$ in Equation (2) of [14] is obtained from Equation (6) and Equation (7) of [15], which were obtained with a code that solves the Boltzmann equations.

Reference [16] obtains k_{fs} by solving the linearized collisionless Boltzmann-Vlasov equation exactly!

An interesting alternative is based on the Jeans length for a collisionless fluid, taken from Lecture Notes by Frank van den Bosch, Theory of galaxy formation, Yale University, fall 2018:

$$\lambda_J \equiv \frac{2\pi}{k_J} = v_{h\text{rms}}(1)\sqrt{\frac{\pi}{G\Omega_m \rho_{\text{crit}} a_{\text{eq}}}}. \tag{15}$$

See Table B for a comparison of these alternative calculations of k_{fs}.

Appendix B. The Mass of Dark Matter Particles

In Reference [4] we use the approximation $m_h v_{h\text{rms}}(1)^2 = 3kT_h(1) = 3ka_{h\text{NR}}^2 T_{h\text{NR}}$ valid for $\mu' \equiv \mu/kT_h \ll 0$. In this **Appendix** we present the exact equations, valid for all μ'. We obtain

$$m_h v_{h\text{rms}}(1)^2 = \frac{8B_{f,b}}{\sqrt{\pi}\Sigma_{f,b}} ka_{h\text{NR}}^2 T_{h\text{NR}}, \tag{16}$$

where $T_{h\text{NR}} \equiv T_h(a_{h\text{NR}})$, and

Table B. Free-streaming cut-off wavenumber k_{fs} for early thermal relics with $m_h = 2500\ \text{eV}$ or $m_h = 70\ \text{eV}$, from several references, and their ratio with respect to k_{fs} from Equation (13). The Table assumes $T_h/T = 0.344$ after e^+e^- annihilation.

Reference	Particle type	m_h	k_{fs}	Ratio
Equation (13)	Fermion	2500 eV	17.8 Mpc^{-1}	ref.
Equation (14)	Fermion	2500 eV	20.3 Mpc^{-1}	1.14
Equation (1.2) of [16]	Fermion	2500 eV	23.5 Mpc^{-1}	1.32
Equation (2) of [14]		2500 eV	12.6 Mpc^{-1}	0.71
Equation (15)		2500 eV	36.0 Mpc^{-1}	2.03
Equation (13)	Boson	2500 eV	21.5 Mpc^{-1}	ref.
Equation (14)	Boson	2500 eV	23.9 Mpc^{-1}	1.11
Equation (1.2) of [16]	Boson	2500 eV	26.2 Mpc^{-1}	1.22
Equation (13)	Fermion	70 eV	0.78 Mpc^{-1}	ref.
Equation (14)	Fermion	70 eV	0.94 Mpc^{-1}	1.21
Equation (1.2) of [16]	Fermion	70 eV	0.66 Mpc^{-1}	0.84
Equation (15)		70 eV	1.01 Mpc^{-1}	1.29
Equation (13)	Boson	70 eV	0.91 Mpc^{-1}	ref.
Equation (14)	Boson	70 eV	1.06 Mpc^{-1}	1.16
Equation (1.2) of [16]	Boson	70 eV	0.73 Mpc^{-1}	0.81

$$B_{f,b} \equiv \int_0^\infty \frac{y^4 \mathrm{d}y}{\exp\left[y^2 - \mu'\right] \pm 1}, \tag{17}$$

(upper sign for fermions, lower sign for bosons). Then Equation (8) of Reference [4] becomes

$$m_h = \left[\frac{64\pi^{3/4}\Omega_c \rho_{\text{crit}} \hbar^3 B_{f,b}^{3/2}}{v_{h\text{rms}}(1)^3 N_{f,b} \Sigma_{f,b}^{5/2}}\right]^{1/4}. \tag{18}$$

and Equation (16) of Reference [4] becomes

$$a_{h\text{NR}} = \frac{\pi^{3/4}\Sigma_{f,b}^{1/6} A_{f,b}^{1/3}}{2B_{f,b}^{1/2}} \frac{v_{h\text{rms}}(1)}{c}. \tag{19}$$

For $\mu = 0$, we obtain for fermions $A_f = 0.09135$, $\Sigma_f = 0.76515$, $B_f = 0.5764$, $m_h c^2 = 1.523 kT_{h\text{NR}}$, $a_{h\text{NR}} = 0.6694 v_{h\text{rms}}(1)/c$, and $0.2941 m_h v_{h\text{rms}}(1)^2 = k a_{h\text{NR}}^2 T_{h\text{NR}}$; and for bosons $A_b = 0.1218$, $\Sigma_b = 2.612$, $B_b = 0.8916$, $m_h c^2 = 0.8139 kT_{h\text{NR}}$, $a_{h\text{NR}} = 0.7269 v_{h\text{rms}}(1)/c$, and $0.6491 m_h v_{h\text{rms}}(1)^2 = k a_{h\text{NR}}^2 T_{h\text{NR}}$. Einstein condensation sets in at $\mu = 0$.

For $\mu/(kT_h) = -1.5$ we obtain for fermions $A_f = 0.0220$, $\Sigma_f = 0.2074$, $B_f = 0.1429$, $m_h c^2 = 1.409 kT_{h\text{NR}}$, $a_{h\text{NR}} = 0.6731 v_{h\text{rms}}(1)/c$, and $0.3216 m_h v_{h\text{rms}}(1)^2 = k a_{h\text{NR}}^2 T_{h\text{NR}}$; and for bosons $A_b = 0.02328$, $\Sigma_b = 0.2432$, $B_b = 0.1547$, $m_h c^2 = 1.315 kT_{h\text{NR}}$, $a_{h\text{NR}} = 0.6768 v_{h\text{rms}}(1)/c$, and

$0.3484 m_h v_{h\text{rms}}(1)^2 = k a_{h\text{NR}}^2 T_{h\text{NR}}$.

For $\mu/(kT_h) = -10.0$ we obtain for both fermions and bosons $A_{f,b} = 4.60 \times 10^{-6}$, $\Sigma_{f,b} = 4.54 \times 10^{-5}$, $B_{f,b} = 3.02 \times 10^{-5}$, $m_h c^2 = 1.366 kT_{h\text{NR}}$, $a_{h\text{NR}} = 0.6747 v_{h\text{rms}}(1)/c$, and $0.3333 m_h v_{h\text{rms}}(1)^2 = k a_{h\text{NR}}^2 T_{h\text{NR}}$.